J Therm Anal Calorim (2012) 107:633–643
DOI 10.1007/s10973-011-1705-4

Effect of different inorganic filler over isothermal and non-isothermal crystallization of polypropylene homopolymer

Vera Alejandra Alvarez · Claudio Javier Pérez

Received: 7 February 2011 / Accepted: 26 May 2011 / Published online: 17 June 2011

Abstract In this study, the effect of several inorganic fillers: silicon oxide (SiO_2), nanoclay (C20A), alumina (Al_2O_3), and calcium carbonate ($CaCO_3$) on the crystallization behavior of polypropylene were analyzed for composites with fixed filler content (5 mass%) prepared by intensive mixing following by compression molding. In addition, for calcium carbonate, which produces the highest increase on toughness, PP grafted with maleic anhydride (PP-g-MA) was added to enhance the compatibility. In that case, different content of particles was used (from 5 to 20 mass%) and the synergic effect of both incorporations was demonstrated. For this purpose, isothermal and non-isothermal crystallization tests were carried out in the bulk (by differential scanning calorimetry). In addition, the spherulitic growth was studied (by optical microscopy). Different models were used to predict the relative degree of crystallinity and several parameters were analyzed. All results indicate that whereas alumina and calcium carbonate acted as nucleating agents, silica and nanoclay displayed an opposite behavior. The full models that take into account the different parameters during cooling under isothermal and non-isothermal conditions were used to construct continuous cooling transformation and time temperature transformation diagrams. Both kind of diagrams provide a fundamental tool to understand the crystallization behavior of studied composites and are useful to determine the processing conditions.

V. A. Alvarez · C. J. Pérez (✉)
Research Institute of Material Science and Technology (INTEMA), Engineering Faculty, National University of Mar del Plata (UNMdP), Av. Juan B. Justo 4302, 7600 Mar del Plata, Argentina
e-mail: cjperez@fi.mdp.edu.ar

Keywords Crystallization · Polypropylene · Modeling · Fillers · Compatibility

Introduction

Natural inorganic fillers like talc, silica, alumina, clay, and calcium carbonate are added to thermoplastics and thermosetting polymers for different applications [1–3]. The use of these additives causes changes in several properties such as heat distortion temperature, hardness, toughness, stiffness, and shrinkage [4, 5]. The effect of filler on the properties of composites strongly depends on its shape, size, aggregate size, and degree of dispersion which is related mainly with the matrix/filler compatibility and the processing technique [6, 7]. One of the polyolefin most used to prepare composites is polypropylene (PP) whose properties depend on the crystalline structure [8]. Many studies related to the crystallization kinetics of PP with various types of fillers such as SiO_2 [8, 9], $CaCO_3$ [2, 10], Al_2O_3 [11], and nanoclay [12–14] have been published. These studies have shown that fillers can either increase or decrease the global crystallization rate of PP. In addition, maleic anhydride grafted PP (PP-g-MA) can be used in order to improve the PP/clay compatibility; in the last case, another effect should be taken into account: the use of PP-g-MA compatibilizer contributes to the retardation of the quiescent isothermal crystallization kinetics [12, 15, 16].

Several authors have demonstrated the nucleating and accelerating effects of nanoclay on the crystallization behavior of semicrystalline polymers in different ways. Several studies were related with experimental parameters such as the increase on the melting and crystallization temperatures or the crystallization rate [8, 9, 13, 17–20]. On the other hand, dissimilar results related with the

applicability of different models are found in the literature: whereas some authors [20] asserted that Avrami and Ozawa are inapplicable and Mo's model is useful to describe the non-isothermal crystallization behavior of nanocomposites; other ones [9] claimed that Avrami's but not Ozawa's was applicable. In addition, diverse results [9, 19, 21] regarding model parameters were found. Another contradiction is related to the clay/matrix compatibility: whereas some works [22] demonstrated that the higher the dispersion degree produce a decrease on the nucleation effect, another ones [19] stated that the higher clay interlayer spacing, due to the increased compatibility, improved the nucleation effect.

In a previous study, the effect of different fillers on the toughness of PP homopolymer was studied. The composite with $CaCO_3$ displayed the highest ductility and toughness, in tensile tests, among all studied materials [23]. The aim of this study was to study and to model the crystallization process (isothermal, non-isothermal, and spherulitic growth) of PP reinforced with different fillers. In addition, the effect filler/matrix compatibility (incorporating PP-g-MA) on the experimental behavior and parameters obtained from several models will be analyzed. Due to the previously explained contradictory results regarding the effect of fillers on crystallization behavior of PP, the main idea of this study was to show the consequence of different fillers with the same PP as matrix.

Experimental

Materials and methods

Isotactic PP (PP 1100N, MFI = 11; T_m = 166 °C) kindly supplied by Petroquímica Cuyo, Argentina, was used as matrix. Four different commercially available additives: Silicon oxide (SiO_2), Aluminum oxide (Al_2O_3), Calcium carbonate ($CaCO_3$) (Sigma-Aldrich), and Cloisite 20A® (C20A, Southern Clay Products Inc., USA) were employed as fillers. They were used as received. Their characteristics are shown in Table 1.

In order to improve the compatibility between PP and $CaCO_3$, 10 mass% of maleic anhydride grafted PP (PP-g-MA) (Epolene E-43 wax, maleic anhydride < 0.7%, Eastman Chemical Company, USA) was also added in the formulation of some composites.

Table 1 Characteristics of the different filler used

Filler	Particle dimensions/nm	Volume fraction/%	Specific density/ g cm^{-3}
SiO_2	10	2.0	2.33
Al_2O_3	<50	1.2	4.00
$CaCO_3$	10.000–30.000	1.6	2.93
C20A	d_{001} = 2.44	2.8	1.77

Composites preparation

The composites were prepared in an intensive mixer (type Brabender) at 180 °C; the speed of rotation and the mixing time were 50 rpm and 10 min, respectively. 5 mass% of different fillers was used. After mixing, 3-mm plaques were compression molded in a hydraulic press for 10 min at 180 °C under a pressure of 50 kg cm^{-2}. Once the effect of fillers was studied, the effect of PP-g-MA incorporation was analyzed by preparing the following materials: 10 mass% of PP-g-MA was incorporated to the neat matrix (PP); 10 mass% of PP-g-MA was incorporated to PP with 5, 10, and 20 mass% of $CaCO_3$ composites.

Transmission electron microscopy (TEM)

Transmission electron microscope JEOL CX II, using an acceleration voltage of 80 kV, was used in order to observe the dispersion of different fillers within the polymer chains. Samples were sectioned in a LKB ultramicrotome with a diamond knife.

Scanning electron microscopy (SEM)

The dispersion of $CaCO_3$ on a microscopic scale was examined using SEM equipment (Philips model JEOL JSM-6460 LV). Specimens were cooled in liquid air and then broken.

Differential scanning calorimeter

DSC Perkin Elmer 7 was used to study the isothermal and non-isothermal crystallization processes. All DSC tests were performed under nitrogen atmosphere. In both cases; a first run was done from room temperature to 200 °C at a heating rate of 10 °C min^{-1}. After that the samples were maintained for 5 min at 200 °C and then: (a) Isothermal crystallization: they were cooled to the crystallization temperature at 30 °C min^{-1}, and maintained at the crystallization temperature for 30 min to let complete crystallization. The material was crystallized in the temperature range of 127–135 °C. Then the samples were heated from the crystallization temperature to 200 °C at 10 °C min^{-1} in order to melt all crystals produced at the crystallization temperature and to find the melting temperature and (b) Non-isothermal crystallization: they were cooled from 200 °C to room temperature at different cooling rates (5, 10, 15, 20, and 30 °C min^{-1}).

Transmission optical microscopy (TOM)

An optical microscopy Leica DM LB, with a hot stage Linkam THMS 600 and a cross polarizer, was used for this study. Samples were prepared by cutting small pieces from films. These samples were heated from room temperature to 200 °C at 10 °C min^{-1}, kept 10 min at 200 °C and then they were quickly cooled to the crystallization temperature (140 °C) and maintained at least 10 min. Polarized light was used in order to observe the spherulites morphology. Pictures of the spherulites were taken at several times and their radii were measured by using a software tool. The time-lapsed frames were recorded in order to determine the spherulitic growth rate.

Results and discussion

The degree of crystallinity was calculated by using the following equation [24]:

$$X_{cr}(\%) = (\Delta H_f / w_{PP} \times \Delta H_{100}) \times 100 \quad (1)$$

where ΔH_f is the experimental heat of fusion, w_{PP} is the PP mass fraction, and ΔH_{100} is the heat of fusion of 100% crystalline PP and its value is 207.1 J g^{-1} [25].

The degree of crystallinity was almost constant (44.8 ± 1.3%) for the matrix and all composites. A similar value and tendency were found by other authors [26, 27]. This is an expected behavior because only a small portion of the added particles have an effect on the nucleation [28, 29] whereas most of them restrict the motion of PP chains; the restricted chains might not crystallize decreasing the crystallinity degree.

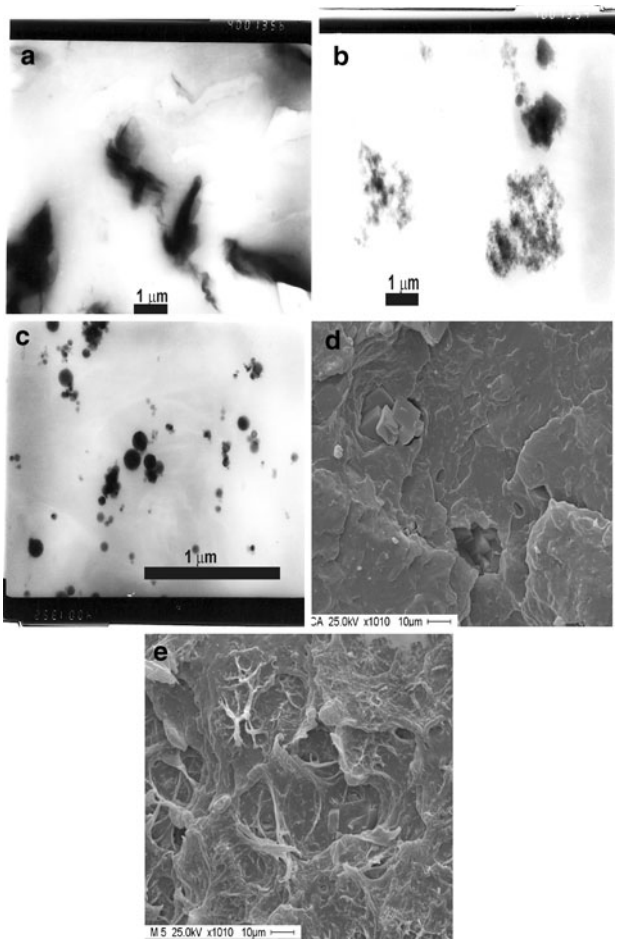

Fig. 1 Electronic micrographics for: **a** PP–5 mass% C20A, **b** PP–5 mass% SiO_2, **c** PP–5 mass% Al_2O_3, **d** PP–5 mass% $CaCO_3$, and **e** PP/10 mass%; PP-g-MA 5 mass% $CaCO_3$. **a**–**c** TEM, **d**, **e** SEM

Bulk-isothermal crystallization process

From the fusion temperature after each crystallization step, the T_m^0 (thermodynamic melting point) was determined by using the Hoffman-Weeks method, extrapolating the experimental points of $T_m = f(T_c)$ plot to the interception with the $T_m = T_c$ plot [30]. According with previous results [31, 32], T_m^0 was practically constant (181.6 ± 2.1 °C) for all materials. This result supports the idea that the particles do not have an important effect on the perfection of PP crystallites. The incorporation of PP-g-MA to the neat matrix did not have any important effect on the theoretical melting point. The same is valid for modified PP-matrix with 5, 10, and 20 mass% of calcium carbonate.

Figure 1 show TEM and SEM micrographs of PP with 5 mass% of different fillers. The dispersion of fillers is not completely homogeneous. As the matrix is hydrophobic and the fillers are hydrophilic, there is necessary to improve the interactions between both. For this purpose, there are two options: one possibility is to functionalize the polymer by the addition of functional oligomers, for example PP-g-MA, and the other one is to modify the fillers. Figure 1e shows a micrograph of PP–10 mass% MA–5 mass% $CaCO_3$. It can be observed that the dispersion was improved due to the incorporation of the compatibilizer.

Overall crystallization rate

Figure 2 show the degree of crystallinity as a function of time (T_c = 129 °C), for the matrix and composites (a) and when the compatibilizer (PP-g-MA) (b) was used. Figure 2a shows that SiO_2 and nanoclay particles delayed the crystallization process [33–36] whereas Al_2O_3 and $CaCO_3$ [37, 38] particles accelerate it.

On the other hand, from Fig. 2b, it is clear that the addition of PP-g-MA delayed the crystallization process [12, 15, 16], but as the quantity of $CaCO_3$ raised, this

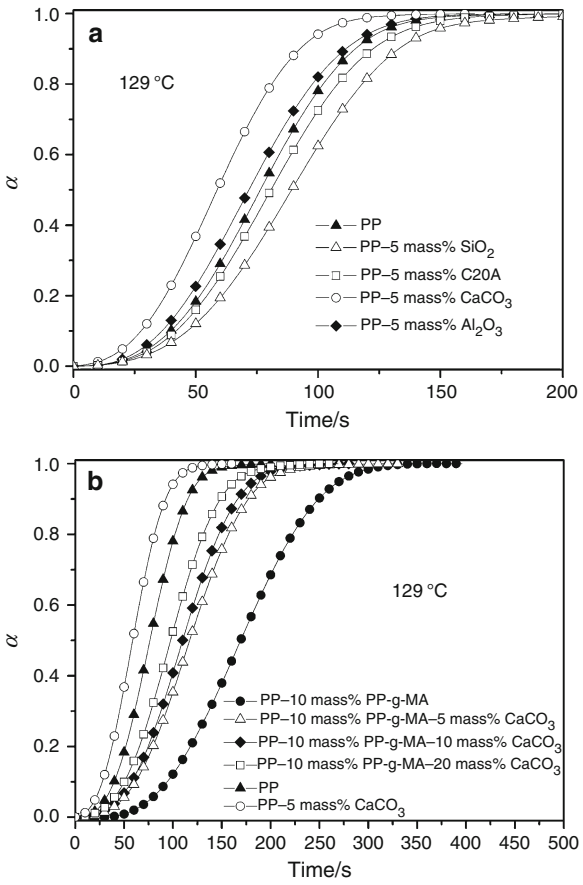

Fig. 2 Relative degree of crystallinity as a function of time at 129 °C for: **a** PP-matrix and composites: PP–5 mass% SiO_2, PP–5 mass% Al_2O_3, PP–5 mass% $CaCO_3$, and PP–5 mass% C20A; **b** PP and PP/10 mass%. PP-g-MA matrices and composites: PP/10 mass% PP-g-MA 5 mass% $CaCO_3$; PP/10 mass% PP-g-MA 10 mass% $CaCO_3$, and PP/10 mass%. PP-g-MA 20 mass% $CaCO_3$

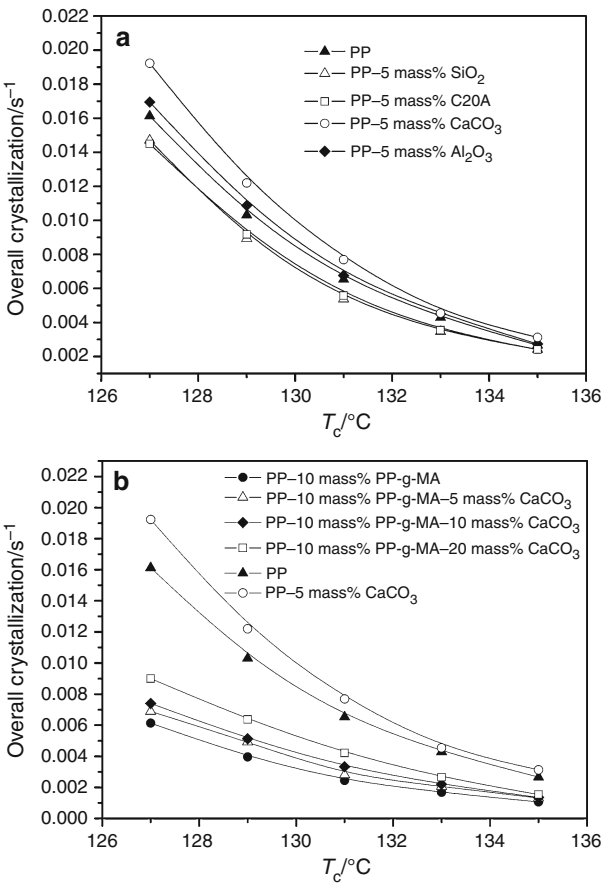

Fig. 3 Overall crystallization rate as a function of crystallization temperature for: **a** PP-matrix and composites: PP–5 mass% SiO_2, PP–5 mass% Al_2O_3, PP–5 mass% $CaCO_3$, and PP–5 mass% C20A. **b** PP and PP/10 mass% PP-g-MA matrices and composites PP/10 mass% PP-g-MA 5 mass% $CaCO_3$; PP/10 mass% PP-g-MA 10 mass% $CaCO_3$, and PP/10 mass% PP-g-MA 20 mass% $CaCO_3$

behavior was changed; because particles accelerate the crystallization process, as it was previously explained.

An approximation of the crystallization rate can be made by calculating the overall crystallization rate ($t_{½}^{-1}$), where $t_{½}$ (half-crystallization time) is the time at which the relative degree of crystallinity (α) approach to 0.5. This parameter is proportional to both the primary nucleation rate and the crystal/spherulite growth.

Figure 3 show the experimental overall crystallization rate (OCR) as a function of crystallization temperature. It can be observed that this parameter decreases as the crystallization temperature becomes higher due to the lower undercooling degree, i.e., the lower crystallization driving force. Some studies [33, 34] have shown the nucleating effect of SiO_2 and clay but for lower nanofiller contents. While the composites with 5 mass% Al_2O_3 and 5 mass% $CaCO_3$ crystallized faster than PP-matrix, because the inorganic particles serve as additional nucleation sites, those with SiO_2 and C20A do it slower which is in accordance with previous analysis. The heterogeneous nucleation effect was lower with the C20A due to the major compatibilization between PP and the clay (the C20A Clay have an organic modifier) [39]. The same behavior was observed when PP-g-MA was introduced. Once again, composites with PP-g-MA and calcium carbonate showed an increased crystallization rate as a function of particle content, and this could be associated with its nucleation effect.

Some authors have reported that at low concentrations the influence of silicate layers, as nucleating agents dominates, while at higher concentrations, the influence of silicate layers as inhibitor of the crystallization becomes predominant [33, 35]. Homminga et al. [33] have attributed this phenomenon to two possible causes: (a) the silicate layers are non-crystallisable barriers for the crystallization of the polymer matrix, which disturb the laterally growing of crystalline lamellae and (b) a decrease in crystal growth rate that is caused by silicate layers through their hindrance on

polymer chain motion. This disturbed crystal growth, however, does not result in visible changes in the semicrystalline stack morphology or the crystal perfection. On the other hand, Krikorian et al. [22] have shown that when the modified clay was highly miscible with the matrix, i.e., exfoliated nanocomposites; the bulk crystallization became slower. Meanwhile, when the miscibility was lower, i.e., intercalated nanocomposites, the bulk crystallization became faster and the degree of crystallinity became higher. Similar behavior was also found other authors [40, 41].

Modeling of isothermal crystallization process

The crystallization kinetics of polymeric matrices under isothermal conditions can be modeled by the Avrami equation [42] which general form is given as:

$$\alpha = 1 - \exp(-k \cdot t^n) \quad (2)$$

where n is the Avrami exponent and k is a rate constant.

The Avrami exponent value depends on two factors: the nucleation mechanism and the geometry of crystal growth. On the other hand, the rate constant k includes nucleation as well as growth-rate parameters. This last parameter usually follows an Arrhenius type relationship with temperature:

$$k = k_0 \cdot \exp(E/(R\Delta T)) \quad (3)$$

where k_0 is the preexponential factor and E is the total activation energy. The parameters of Avrami equation were calculated in the range of α between 0.1 and 0.9. The obtained values are summarized in Table 3, whereas average values for n are included in Table 2. The average value of n was equal to 2.93 ± 0.15 [43, 44], indicating a three-dimensional growth.

Table 2 Parameters of isothermal crystallization for different materials studied

	OCR experimental	OCR predicted	$n_{average}$	E_a/kJ mol^{-1}	X_c/%
Matrix					
PP	0.013	0.013	2.97 ± 0.06	594	45.4
Effect of particles					
PP 5.0 mass% SiO_2	0.011	0.012	2.99 ± 0.07	655	43.6
PP 5.0 mass% Al_2O_3	0.014	0.013	2.76 ± 0.12	514	40.6
PP 5.0 mass% $CaCO_3$	0.014	0.014	2.76 ± 0.15	572	
PP 5.0 mass% C20A	0.012	0.013	2.85 ± 0.09	637	43.5
Effect of PP-g-MA					
PP 10 mass% PP-g-MA	0.006	0.0058	3.05 ± 0.12	601	43.5
PP 10 mass% PP-g-MA–5 mass% $CaCO_3$	0.008	0.0085	3.05 ± 0.14	552	43.0
PP 10 mass% PP-g-MA–10 mass% $CaCO_3$	0.009	0.009	3.04 ± 0.12	542	39.0
PP 10 mass% PP-g-MA–20 mass% $CaCO_3$	0.010	0.0095	3.08 ± 0.17	528	36.4

Table 3 Parameters of Avrami equation for matrix and composites as a function of crystallization temperature

Temperature/°C	127		129		131		133		135	
	n	k ($\times 10^6$)	n	k ($\times 10^6$)	n	k ($\times 10^6$)	n	k ($\times 10^6$)	n	k ($\times 10^6$)
Matrix										
PP	2.9	3.8	2.9	2.1	3.0	1.05	3.05	0.54	3.0	0.26
Effect of particles										
PP 5.0 mass% SiO_2	2.9	3.2	2.9	1.5	2.9	0.94	3.0	0.49	3.1	0.25
PP 5.0 mass% Al_2O_3	2.7	3.7	2.8	1.8	2.8	0.97	2.9	0.51	3.0	0.24
PP 5.0 mass% $CaCO_3$	2.6	4.3	2.7	2.5	2.8	1.3	2.8	0.76	2.9	0.47
PP 5.0 mass% C20A	2.6	4.0	2.7	2.1	2.8	1.2	2.9	0.57	3.0	0.31
Effect of PP-g-MA										
PP 10 mass%. PP-g-MA	2.9	0.42	3.1	0.21	3.1	0.11	3.0	0.06	3.1	0.03
PP 10 mass% PP-g-MA–5 mass% $CaCO_3$	2.9	1.00	2.9	0.60	3.1	0.27	3.1	0.14	3.2	0.08
PP 10 mass% PP-g-MA–10 mass% $CaCO_3$	2.9	1.30	2.9	0.72	3.1	0.35	3.2	0.17	3.1	0.08
PP 10 mass% PP-g-MA–20 mass% $CaCO_3$	3.0	1.60	2.8	1.00	3.1	0.46	3.1	0.25	3.3	0.12

Table 4 Parameters of non-isothermal crystallization for all studied materials

	ΔT_p/°C 10 °C min^{-1}	$t_{1/2}$/s 10 °C min^{-1}	E_a (kisinger)/ kJ mol^{-1}	Ozawa		Avrami		Mo	
				$K(T)$	m	Z_c	n	b	$F(T)$
PP	60.8	71	217	6300	3.4	0.023	8.3	1.18	15.5
PP 5.0 mass% SiO_2	59.7	123	232	2900	3.3	0.016	9.3	1.05	13.1
PP 5.0 mass% Al_2O_3	60.7	70	202	7100	3.5	0.080	5.8	1.20	13.6
PP 5.0 mass% $CaCO_3$	60.7	66	205	8800	3.5	0.043	7.1	1.17	13.5
PP 5.0 mass% C20A	60.9	125	219	4700	3.2	0.020	8.8	1.11	13.7

$\Delta T_p = T_m^0 - T_p$. T_p peak temperature at cooling rate of 10 °C min^{-1}, $t_{1/2}$ 10 °C m^{-1}: half-crystallization time at cooling rate of 10 °C min^{-1}, E_a activation energy for the transport of the macromolecular segments to the growing surface (Kissinger method), *Ozawa* parameters of Ozawa's model obtained at $T = 118$ °C, *Avrami* parameters of Avrami's model obtained at 10 °C min^{-1}, *Mo* parameters of Mo's model obtained for $\alpha = 0.6$

In all cases, the rate constant, k, decreased with the increase on the crystallization temperature [9]. In addition, the parameter k, increased for accelerating particles ($CaCO_3$ and Al_2O_3) whereas decreased for retardant ones (SiO_2 and C20A). On the other hand, the addition of PP-g-MA produced a decrease on k which is related with a slower crystallization process. The results indicate that this parameter (k) could be useful to understand the nucleation and fastening effect of filler because a higher value of k implies a higher nucleation effect.

The preexponential factors (k_0) and activation energies (E_a) were obtained from a typical nonlinear regression method. The values of activation energies (for an average n of 2.93) are also included in Table 2**.** The addition of Al_2O_3 and $CaCO_3$ produced a decrease on the E_a whereas the incorporation of SiO_2 and clay produced an increase on this parameter. On the other hand, the trend with PP-g-MA and the posterior incorporation of $CaCO_3$ was the expected one: activation energy increased (with PP-g-MA) and the decreased (with increasing the content of calcium carbonate).

Non-isothermal crystallization analysis

From the crystallization curves, at different cooling rates, some data useful to describe their non-isothermal crystallization behavior, such as the exothermic peak temperature (T_p) and the onset crystallization temperature (T_o) can be obtained. There were no important differences on the undercooling degree for different fillers (see Table 4). It was observed that, in all cases, ΔT_p increased with increased cooling rate because more nuclei became active at lower temperatures [45], conducting to smaller spherulites during the heterogeneous nucleation process. ΔT_p and also $t_{1/2}$ for a cooling rate of 10 °C min^{-1} are summarized in Table 4. The most relevant parameters of used models are also included in that table. It can be observed that, for a fixed cooling rate, the half-crystallization times for composites with alumina and calcium carbonate were lower than for the neat PP implying that the addition of these fillers can accelerate the overall crystallization process [8] whereas the values for silica and nanoclay were higher. On the other hand, $t_{1/2}$ clearly increased with PP-g-MA addition but then decreased as a function of $CaCO_3$ content.

Modeling of non-isothermal crystallization process

The relative degree of crystallinity as a function of temperature, $\alpha(T)$, can be calculated as:

$$\alpha(T) = \int_{T_o}^{T} ((dH_c/dT)dT) \Big/ \int_{T_o}^{T_\infty} ((dH_c/dt)dT) \quad (4)$$

where T_o and T_∞ represent the onset and final crystallization temperatures, respectively and H_c is the crystallization enthalpy. Assuming that non-isothermal crystallization process may be composed by infinitesimally small isothermal crystallization steps, Ozawa [46] extended the Avrami equation for the non-isothermal case as follows:

$$1 - \alpha = \exp(-K(T)/\phi^m) \quad (5)$$

where $K(T)$ is a function of cooling rate, ϕ is the cooling rate, and m is the Ozawa exponent that depends on the crystal growth. Equation 6 can be transformed in:

$$\ln(-\ln(1-\alpha)) = \ln(K(T)) - m\ln\phi \quad (6)$$

By plotting ln (−ln (1 − α)) versus lnϕ at a given temperature, a straight line should be obtained being possible to calculate $K(T)$ and m.

Another method, developed by Mo [47], can be also employed to describe the non-isothermal crystallization process, for which physical variables are: the relative degree of crystallinity (X_t), the cooling rate (ϕ), and the crystallization temperature (T_c). Both equations can be related as follows:

$$\ln Zt + n\ln t = \ln K(T) - m\ln\phi \quad (7)$$

Rearranging the previous equation at a given crystallinity X_t

$$\ln\phi = \ln F(T) - a\ln t \quad (8)$$

where $F(T) = [K(T)\cdot Z_t^{-1}]^{m-1}$ refers to the cooling rate, which must be chosen within unit crystallization time when the measured system amounts to a certain degree of crystallinity, $a = n\cdot m^{-1}$, the ratio of Avrami exponent to Ozawa exponent.

Kissinger [48] have suggested a method to determine the activation energy for the transport of the macromolecular segments to the growing surface, ΔE_T, by calculating the variation of temperature peak (T_p) with the cooling rate ϕ. The equation is expressed as follows:

$$\mathrm{d}\left[\ln\left(\phi/T_p^2\right)\right]\Big/\mathrm{d}\left(1/T_p\right) = -\Delta E/R \quad (9)$$

where R is the gas constant. The values of $\ln(\phi\,(T_p^2)^{-1})$ were plotted as a function of T_p^{-1} and good relations were obtained. From these plots, the activation energy for the transport of the macromolecular segments to the growing surface (Kissinger's method) was estimated and the values are also included in Table 4. The results of activation energies of non-isothermal melt crystallization also show the nucleating effect of alumina and calcium carbonate and the retardant effect of SiO_2 and C20A, as it was previously discussed. Other authors [18, 49] have found a similar trend on activation energy. In the case of PP modified with PP-g-MA, the obtained values were lower than that of the matrix but the same may be higher because the retardant effect, the crystallization ability of PP-g-MA is lower than that of PP because of the lower chain regularity. Moreover, PP-g-MA with low maleic anhydride content is compatible with PP. Therefore, the crystallization rate in the PP/PP-g-MA blends is reduced due to the presence of the compatible polymeric additive with lower crystallization ability [15]. So, the observed trend may result from a decrease in the viscosity when the PP is blended with the PP-g-MA, decreasing the restriction on the polymer chains motion. There are two simultaneous effects with the addition of $CaCO_3$: the $CaCO_3$ is a nucleating agent (E_a decrease) but the viscosity increased (E_a increase). The global result shows that the E_a is almost constant.

Results of the application of Ozawa's model are shown in Table 5. The value of $K(T)$ increased as the crystallization temperature decreased (higher driving force for the crystallization process) for the matrix and PP–5 mass% $CaCO_3$ and PP–5 mass% Al_2O_3 composites. The values were higher for the composites than for the matrix, at any given crystallization temperature, indicating that composites crystallized faster than the pure matrix, which is also coincident with all previous results. On other hand, the contrary effect is observed in the composites PP–5 mass% SiO_2 and PP–5 mass% C20A.

Table 5 Ozawa's parameters for different studied materials

T/°C	116		118		120	
Sample	m	$K(T)$	m	$K(T)$	m	$K(T)$
PP	3.1	7500	3.4	6300	3.7	6000
Effect of particles						
PP 5 mass% SiO_2	2.7	1000	3.3	2900	3.5	4200
PP 5 mass% Al_2O_3	3.3	12600	3.5	7080	3.6	6470
PP 5 mass% $CaCO_3$	3.4	18900	3.5	8800	3.8	7100
PP 5 mass% C20A	2.7	1800	3.2	4700	3.9	5900

The parameters obtained by using Avrami's model are displayed in Table 6. Z_t and n do not have the same physical meaning than in isothermal crystallization because under non-isothermal crystallization the temperature changes continuously affect the nuclei formation and spherulite growth rate. The corrected crystallization constant (Z_c) increased as a function of cooling rate. The values of Z_c are smaller for PP–5 mass% SiO_2 and PP–5 mass% C20A composites than for the matrix (retardant effect) meanwhile composites PP–5 mass% Al_2O_3 and PP–5 mass% $CaCO_3$ displayed the opposite effect. At fixed cooling rate, n decreased for the composites that showed a nucleating effect.

The combination of Ozawa and Avrami models leads to Mo analysis, whose parameters are summarized in Table 7. $F(T)$ and b increased with the relative degree of crystallinity (α). No significant tendency was observed with different fillers. Although this last model correctly represents the experimental crystallization curves for all composites, the parameters do not appear to be adequate to establish the nucleating or retarding effect of the fillers.

It is possible to obtain global kinetic model that allow predicting the crystallinity development under any cooling conditions, such as real industrial processing conditions. That is a very important tool to design the processing steps of a semicrystalline polymer. That full model is also useful for the construction of phase diagrams. These diagrams allow estimating the nucleation and growth of crystals for specific cooling conditions. Two types of diagrams are commonly used: (1) TTT: Time–Temperature–Transformations plots (isothermal processes) and (2) CCT: Continuous Cooling Transformations plots (at constant cooling rate) in which the crystallinity is related with time and temperature at constant cooling rate. This approach permits the knowledge of the entire crystallization process [50, 51]. CCT and TTT plots of studied materials are shown in Fig. 4 (a: composites with different fillers and b: composites modified with PP-g-MA). The curves for the relative

Table 6 Avrami's parameters for the different studied materials

ϕ	5		10		15		20		30	
Sample	n	Z_c	n	Z_c	n	Z_c	n	Z_c	n	Z_c
PP	7.7	5e−4	8.3	0.023	8.2	0.10	7.5	0.23	7.1	0.44
Effect of particles										
PP 5 mass% SiO_2	9.7	4e−5	9.3	0.016	9.0	0.09	8.6	0.20	7.6	0.44
PP 5 mass% Al_2O_3	6.9	1e−3	5.8	0.080	5.6	0.22	5.5	0.35	4.6	0.58
PP 5 mass% $CaCO_3$	7.4	7e−4	7.1	0.043	6.3	0.19	6.4	0.30	6.2	0.49
PP 5 mass% C20A	9.0	4e−4	8.8	0.02	8.4	0.08	8.2	0.17	7.3	0.43

Table 7 Mo's parameters for the different studied materials

	0.2		0.4		0.6		0.8	
Sample	b	$F(T)$	b	$F(T)$	b	$F(T)$	b	$F(T)$
PP	1.15	12.5	1.16	14.1	1.18	15.5	1.21	17.5
Effect of particles								
PP 5 mass% SiO_2	1.02	11.0	1.05	12.1	1.05	13.1	1.10	14.4
PP 5 mass% Al_2O_3	1.13	10.3	1.15	11.9	1.20	13.6	1.27	15.9
PP 5 mass% $CaCO_3$	1.13	10.6	1.16	12.2	1.17	13.5	1.21	15.2
PP 5 mass% C20A	1.07	11.0	1.10	12.5	1.11	13.7	1.15	15.5

degree of crystallinity of 0.5 (CCT) and 0.9 (TTT) are plotted as a function of time. Each point on these curves has been obtained by integrating the full model (nucleation and growth) at a given constant temperature or at a constant cooling rate. Both diagrams of composites with different fillers reveal that the same relative crystallinity degree is reached at lower time for 5 mass% $CaCO_3$ and 5 mass% Al_2O_3 composites, demonstrating that these particles act as nucleating agent during the crystallization process. An opposite effect was observed for 5 mass% SiO_2 and 5 mass% C20A composites. On the other hand, diagrams of composites with PP-g-MA, disclosed that PP modified with 10 mass% PP-g-MA present the highest retarding effect (longest time is required to reach the same relative crystallinity degree). Then, this effect decreased with the continuous addition of $CaCO_3$.

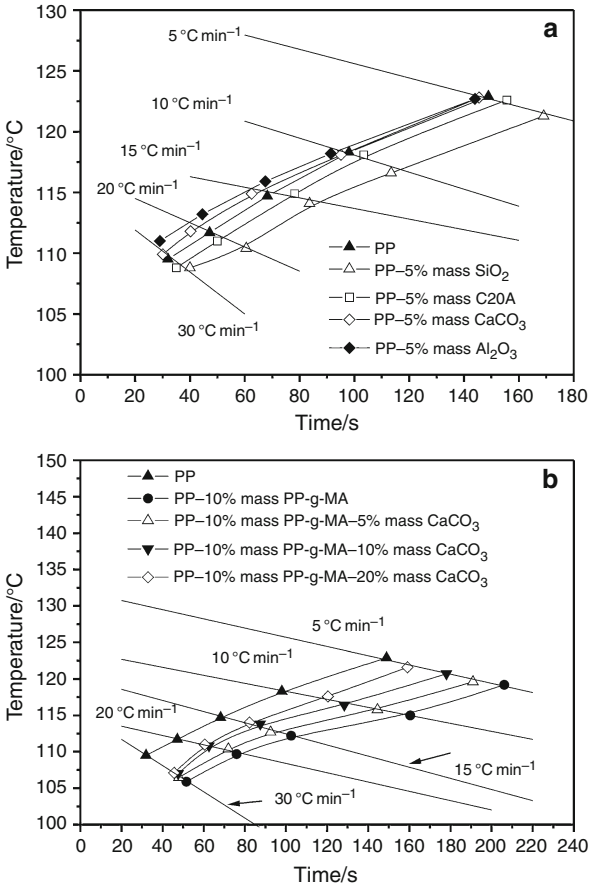

Fig. 4 CTT and TTT diagrams for: **a** PP-matrix and composites: PP–5 mass% SiO_2, PP–5 mass% Al_2O_3, PP–5 mass% $CaCO_3$ and PP–5 mass% C20A. **b** PP and composites: PP/10 mass% PP-g-MA 5 mass% $CaCO_3$; PP/10 mass% PP-g-MA 10 mass% $CaCO_3$ and PP/10 mass% PP-g-MA 20 mass% $CaCO_3$

Spherulitic growth

Figure 5 shows the micrographs of growing spherulites for PP modified with 10 mass% PP-g-MA at 140 °C and two different times (360 and 720 s). The morphology of spherulites (not shown) was quite similar for all studied materials. Table 8 summarized the number of growing nucleus and the spherulites radius at the same time and undercooling degree for matrix and selected composites. The number of growing nucleus was higher for composites with 5 mass% Al_2O_3 and 5 mass% $CaCO_3$, and it can be attributed to the nucleating effect of the particles which in turns coincides with the studies carried out with DSC. On the other hand, the opposite effect was obtained for composites with 5 mass% C20A and 5 mass% SiO_2. A similar behavior was found for the spherulite radius of composites (140 °C, 360 s). In the case of composites modified with

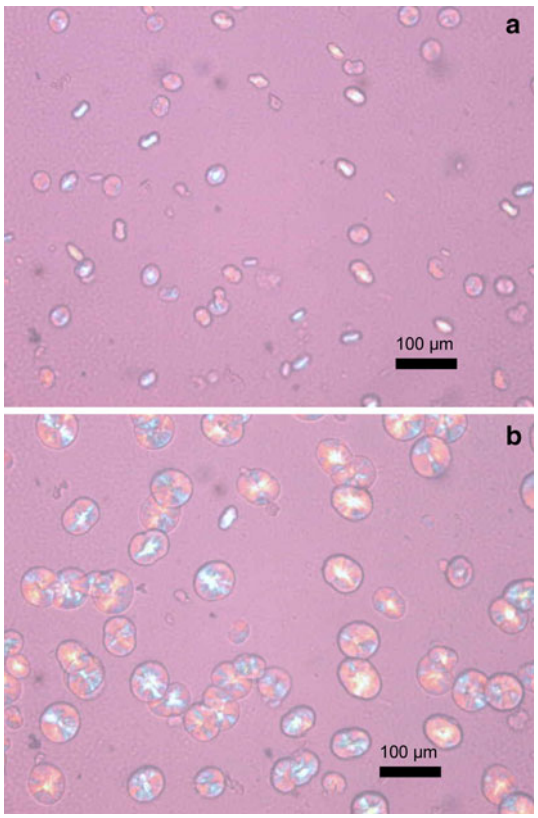

Fig. 5 Spherulites morphology of PP–10 mass% PP-g-MA crystallized at 140 °C for different times: **a** 360 and **b** 720 s

PP-g-MA, the number of growing nucleus notoriously decreased (due to the restriction and delaying of the crystallization) but increased as a function of the content of $CaCO_3$.

The spherulites radius as a function of time for the matrix and composites, at the same undercooling degree, were plotted. At least eight spherulites were measured for each test. It was observed that the spherulite radius increased linearly with the time in all cases. This behavior was observed at all undercooling degrees and indicated that the growth rate is independent of the spherulites size. The spherulitic growth rate was calculated as $G = \mathrm{d}R/\mathrm{d}t$ which is the slope of the experimental radius versus time curve at each temperature. The obtained values (at $T_c = 140$ °C) are also included in Table 8. The spherulitic growth rate increased by the incorporation of the nucleating agent ($CaCO_3$ and Al_2O_3) and decreased by the incorporation of the retarding ones (SiO_2 and C20A). Comparing composites with PP-g-MA, it can be observed that the spherulitic growth rate increased with the increase on the content of $CaCO_3$. In addition, in all cases, the spherulitic growth rate increased with the undercooling degree.

Table 8 Parameters of spherulitic growth

Sample	Growing nucleus number/mm^{-2} 140 °C, 360 s	Spherulites radius/μm 140 °C, 360 s	G/μm s^{-1} 140 °C
Matrix			
PP	130 ± 35	17 ± 2	0.040 ± 0.01
Effect of particles			
PP–5 mass% SiO_2	125 ± 11	11 ± 2.1	0.031 ± 0.01
PP–5 mass% Al_2O_3	210 ± 12	20 ± 2.2	0.042 ± 0.003
PP–5 mass% $CaCO_3$	139 ± 12	18 ± 3	0.047 ± 0.004
PP–5 mass% C20A	100 ± 12	15 ± 3.2	0.037 ± 0.004
Effect of PP-g-MA			
PP 10 mass%. PP-g-MA	25 ± 3	13 ± 2.1	0.030 ± 0.003
PP 10 mass% PP-g-MA–5 mass% $CaCO_3$	52 ± 6	11 ± 2.4	0.032 ± 0.005
PP 10 mass% PP-g-MA–10 mass% $CaCO_3$	67 ± 7	13 ± 1.4	0.035 ± 0.004
PP 10 mass% PP-g-MA–20 mass% $CaCO_3$	71 ± 8	11 ± 3.2	0.037 ± 0.003

Conclusions

The effect of several inorganic fillers: silica (SiO_2), nanoclay (C20A), alumina (Al_2O_3), and calcium carbonate ($CaCO_3$) on the crystallization behavior of PP was established. All experimental and models parameters results indicate that whereas alumina and calcium carbonate acted as nucleating agents, silica and nanoclay displayed the opposite behavior. PP grafted with maleic anhydride (PP-g-MA) produced an increase on the compatibility but with a clear reduction on the crystallization rate due to the presence of the compatible additive with lower crystallization ability. The subsequent addition of calcium carbonate produced a competitive effect: the retardant one associated with PP-g-MA and the accelerating one related with the particles being the final behavior dependent on the balance of both outcomes.

The spherulitic growth rate increased for the nucleating agents ($CaCO_3$ and Al_2O_3) but decreased through the retarding ones (SiO_2 and C20A). The spherulitic growth increased with the content of $CaCO_3$ for composites with PP-g-MA. CCT and TTT diagrams were constructed for all systems. These diagrams allow the determination of the crystallinity degree for different processing conditions. This information is very useful for the design and optimization of

processing steps. Besides, these diagrams confirmed the nucleating and retarding effect of different fillers in accordance with all previous analysis.

The efficiency of filler on crystal nucleation and growth seems to be related with the filler-matrix compatibility.

Acknowledgements The authors would like to acknowledge the financial support of the National Research Council of Argentina (CONICET) and the ANPCyT.

References

1. Ray S, Okamoto M. Polymer/layered nanocomposites: a review from preparation to processing. Prog Polym Sci. 2003;28:1539–641.
2. Chan CM, Wu JS, Li JX, Cheung YK. Polypropylene/calcium carbonate nanocomposites. Polymer. 2002;43:2981–92.
3. Zhou Y, Rangari V, Mahfuz H, Jeelani S, Mallick PK. Experimental study on thermal and mechanical behavior of polypropylene, talc/polypropylene and polypropylene/clay nanocomposites. Mat Sci Eng A. 2005;402:109–17.
4. Gong G, Xie BH, Yang W, Li ZM, Lai SM, Yang MB. Plastic deformation behavior of PP/calcium carbonate composites with and without maleic anhydride grafted polypropylene incorporated using the essential work of fracture method. Polym Test. 2006;25:98–106.
5. Velasco JI, Morhain C, Martinez AB, Rodríguez Pérez MA, Saja JA. The effect of filler type, morphology and coating on the anisotropy and microstructure heterogeneity of injection-moulded discs of polypropylene filled with aluminium and magnesium hydroxides. Part 1. A wide-angle X-ray diffraction study. Polymer. 2002;43:6805–11.
6. Zhang J, Ding QJ, Zhou NL, Li L, Ma ZM, Shen J. Studies on crystal morphology and crystallization kinetics of polypropylene filled with $CaCO_3$ of different size and size distribution. J Appl Polym Sci. 2005;101:2437–44.
7. Seo Y, Kim J, Kim KU, Kim YC. Study of the crystallization behaviors of PP and maleic anhydride grafted PP. Polymer. 2000;41:2639–46.
8. Jain S, Goossens H, van Duin M, Lemstra P. Effect of in situ prepared silica nano-particles on non-isothermal crystallization of polypropylene. Polymer. 2005;46:8805–18.
9. Papageorgiou G, Achilias D, Bikiaris D, Karayannidis G. Crystallization kinetics and nucleation activity of filler in polypropylene/surface-treated SiO_2 nanocomposites. Thermochim Acta. 2005;427:117–28.
10. Yang K, Yang Q, Li G, Sun Y, Feng D. Morphology and mechanical properties of polypropylene/calcium carbonate nanocomposites. Mater Lett. 2006;60:805–9.
11. Li RKY, Zhao H. Crystallization, mechanical and fracture behaviors of spherical alumina-filled PP nanocomposites. J Polym Sci Polym Phys. 2005;43:3652–64.
12. Perez CJ, Alvarez VA. Overall crystallization behavior of polypropylene–clay nanocomposites; effect of clay content and polymer/clay compatibility on the bulk crystallization and spherulitic growth. J Appl Polym Sci. 2009;114:3248–60.
13. Liu X, Wu Q. PP/clay nanocomposites prepared by grafting-melt intercalation. Polymer. 2001;42:10013–20.
14. Olewnik E, Garman K, Czerwinski W. Thermal properties of new composites based on nanoclay, polyethylene and polypropylene. J Therm Anal Calorim. 2010;101:323–9.
15. Menyhard A, Faludi G, Varga J. β-crystallization tendency and structure of polypropylene grafted by maleic anhydride and its blends with isotactic polypropylene. J Therm Anal Calorim. 2008;93:937–45.
16. Svoboda P, Zeng C, Wang H, Lee J, Tomasko DL. Morphology and mechanical properties of polypropylene/organoclay nanocomposites. J Appl Polym Sci. 2002;85:1562–70.
17. Raka L, Bogoeva G, Loos J. Characterization of polypropylene/layered silicate nanocomposites prepared by single-step method Medellin RFJ. J Therm Anal Calorim. 2010;100:629–39.
18. Xu W, Ge M, He P. Nonisothermal crystallization of polypropylene/montmorillonite nanocomposites. J Polym Sci B Polym Phys. 2002;40:408–14.
19. Xu W, Liang G, Zhai H, Tang S, Hang G, Pan W. Preparation and crystallization of PP/PP-g-MAH/Org-MMT nanocomposite. Eur Polym J. 2003;39:1467–74.
20. Yuan Q, Misra RDK. Impact fracture behavior of clay-reinforced PP nanocomposites. Polymer. 2006;47:4421–33.
21. Li J, Zhou C, Wang G, Tao Y, Liu Q, Li Y. Isothermal and nonisothermal crystallization kinetics of elastomeric polypropylene. Polym Test. 2002;21:583–9.
22. Krikorian V, Pochan DJ. Unusual crystallization behavior of organoclay reinforced poly(L-lactic acid) nanocomposites. Macromolecules. 2004;37:6480–91.
23. Pérez E, Alvarez V, Perez CJ, Bernal C, Tensile and fracture behavior of polypropylene filled with rigid particles. J Appl Polym Sci.
24. Yam WY, Ismail J, Kammer HW, Schmidt H, Kummerlöwe C. Polymer blends of poly(ε-caprolactone) and poly(vinyl methyl ether)—thermal properties and morphology. Polymer. 1999;40:5545–52.
25. Bu HS, Cheng SZD, Wunderlich B. Addendum to the thermal properties of polypropylene. Die Makromol Chem Rapid Commun. 1988;9:75–7.
26. Borsig E, Ujhelyiová A, Mlynarcíková Z, Kaemfer D, Mülhaupt R, Marcincin A, Berek D. DSC study of sindiotactic polypropylene/organoclay nanocomposite fibers: crystallization and melting behavior. Int J Polym Mater. 2007;56:771–8.
27. Li J, Ton-That MT, Leelapornpisit W, Utracki LA. Melt compounding of polypropylene-based clay nanocomposites. Polym Eng Sci. 2007;47:1447–58.
28. Jiang S, Ji X, An L, Jiang B. Confined crystallization behavior of PCL in organic-inorganic hybrid system. Acta Polym Sin. 2000;4:452–6.
29. Cheng Y, Xu M. Comparison of methods for characterizing the effects of nucleating agents on the process of polymer crystallization. Acta Polym Sin. 1998;5:671–8.
30. Hoffman JD, Davis GT, Lauritzen JI. New explanation for chain folding in polymers. In: Hannay NB, editors. Treatise on Solid State Chemistry. Vol 3. Chap 7. New York: Plenum press; 1976.
31. Yamada K, Hikosaka M, Toda A, Yamazaki S, Tagashira K. Equilibrium melting temperature of isotactic polypropylene with high tacticity: 1. Determination by differential scanning calorimetry. Macromolecules. 2003;36:4790–801.
32. Maiti P, Nam PH, Okamoto M, Hasegawa N, Usuki A. Influence of crystallization on intercalation, morphology and mechanical properties of polypropylene/clay nanocomposites. Macromolecules. 2002;35:2042–9.
33. Fornes TD, Paul DR. Crystallization behavior of nylon 6 nanocomposites. Polymer. 2003;44:3945–61.
34. Perez CJ, Vazquez A, Alvarez VA. Isothermal crystallization of layered silicate/starch-polycaprolactone blend nanocomposites. J Therm Anal Calorim. 2008;91:749–57.
35. Homminga D, Goderis B, Dolbnya I, Reynaers H, Groenincks G. Crystallization behavior of polymer/montmorillonite nanocomposites. Part I. Intercalated poly(ethylene oxide)/montmorillonite nanocomposites. Polymer. 2005;46:11359–65.

36. Yang F, Ou Y, Yu Z. Polyamide 6/silica nanocomposites prepared by in situ polymerization. J Appl Polym Sci. 1998;69:355–61.
37. Huang Y, Chen G, Yao Z, Li H, Wu HY. Non-isothermal crystallization behavior of polypropylene with nucleating agents and nano-calcium carbonate. Eur Polym J. 2005;41:2753–60.
38. Avella M, Cosco S, Di Lorenzo ML, Di Pace E, Errico ME, Gentile G. Nucleation activity of nanosized $CaCO_3$ on crystallization of isotactic polypropylene, in dependence on crystal modification, particle shape, and coating. Eur Polym J. 2006;42:1548–57.
39. Ludueña L, Alvarez V, Vazquez A. Crystallization of polycaprolactone-clay nanocomposites. J Appl Polym Sci. 2008;109:3148–56.
40. Somwangtharanoj A, Lee E, Solomon M. Early stage quiescent and flow-induced crystallization of intercalated polypropylene nanocomposites by time-resolved light scattering. Macromolecules. 2003;36:2333–8.
41. Pérez CJ, Alvarez VA, Stefani PM, Vázquez A. Non-isothermal crystallization of mater Bi-Z/CLAY nanocomposites. J Therm Anal Calorim. 2007;88:825–32.
42. Cebe P, Hong SD. Crystallization behaviour of poly(ether-ether-ketone). Polymer. 1986;27:1183–92.
43. Wei Z, Zhang W, Chen G, Liang J, Yang S, Wang P, Liu L. Crystallization and melting behavior of isotactic polypropylene nucleated with individual and compound nucleating agents. J Therm Anal Calorim. 2010;102:775–83.
44. Wu CL, Zhang MQ, Rong MZ, Friedrich K. Silica nanoparticles filled polypropylene: effects of particle surface treatment, matrix ductility and particle species on mechanical performance of the composites. Comp Sci Technol. 2005;65:635–45.
45. Di Lorenzo ML, Silvestre C. Non-isothermal crystallization of polymers. Prog Polym Sci. 1999;24:917–50.
46. Ozawa T. Kinetics of non-isothermal crystallization. Polymer. 1971;12:150–8.
47. Liu TX, Mo ZS, Wang SE, Zhang HF. Nonisothermal melt and cold crystallization kinetics of poly(aryl ether ketone). Polym Eng Sci. 1997;37:568–76.
48. Kisinger HE. Variation of peak temperature with heating rate in differential thermal analysis. J Res Natl Bur Stand. 1956;57:217–24.
49. Wang L, Sheng J. Nonisothermal crystallization kinetics of polypropylene/attapulgite nanocomposites. J Macromol Sci B Phys. 2005;44:31–42.
50. Long Y, Shanks RA, Stachurski ZH. Kinetics of polymer crystallization. Prog Polym Sci. 1995;20:651–701.
51. Hubert L, David L, Seguela R, Vigier G, Degoulet C, Germain Y. Physical and mechanical properties of polyethylene for pipes in relation to molecular architecture. I. Microstructure and crystallization kinetics. Polymer. 2001;42:8425–34.